

Supplementary Information for “Rashba spin splitting and anomalous spin textures in the bulk ferroelectric oxide perovskite KIO_3 ”

Sajjan Sheoran*, Manish Kumar, Preeti Bhumla, Saswata Bhattacharya†
Department of Physics, Indian Institute of Technology Delhi, New Delhi 110016, India
(Dated: February 23, 2022)

I. COORDINATE SYSTEMS

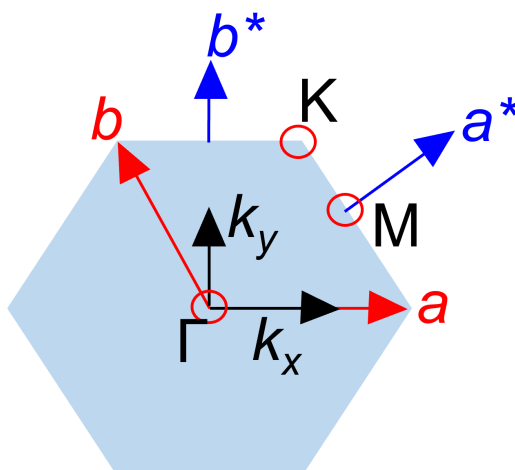


Figure S1: 2D Brillouin zone in $k_x - k_y$ plane ($k_z = 0$) containing the Γ , M and K points. \mathbf{a} and \mathbf{b} are the lattice vectors, while \mathbf{a}^* and \mathbf{b}^* are the reciprocal lattice vectors. Here, x and y directions show the orthogonal reciprocal cartesian vectors k_x and k_y , respectively.

The orientation of the lattice vectors, reciprocal lattice vectors, wave vectors and high symmetry path are shown in Fig. S1. For simplicity, we have added only the $k_x - k_y$ plane containing k -points M, Γ and K, which are used for computing spin textures and spin splitting. \mathbf{a} and \mathbf{b} are the lattice vectors, while \mathbf{a}^* and \mathbf{b}^* are the reciprocal lattice vectors. The angles between lattice vectors and reciprocal lattice vectors are 120° and 60° , respectively. Here, x and y directions show the orthogonal wave vectors k_x and k_y , respectively. The $\Gamma - \text{K}$ direction is symmetrically same as k_x , which leads to band structures computed along $\Gamma - \text{K}$ coincides with k_x . Similarly, $\Gamma - \text{M}$ direction is same as k_y . We have used reciprocal cartesian basis i.e., k_x and k_y to compute spin textures and spin splitting. The lattice vector \mathbf{c} is perpendicular to \mathbf{a} and \mathbf{b} , pointing out of the page. The wave vector k_z is perpendicular to k_x and k_y . The reciprocal lattice vector \mathbf{c}^* , k_z and $\Gamma - \text{A}$ point along the same direction.

* sajjan@physics.iitd.ac.in [SS]

† saswata@physics.iitd.ac.in [SB]

II. HEXAGONAL DISTORTION UNDER STRAIN

Increasing the out-of-plane lattice parameter from 7.7 Å to 8.5 Å decreases the in-plane lattice parameters (i.e. a and b) and accordingly, the c/a ratio also increases. Figure S2 shows the variation of a and c/a as a function of c .

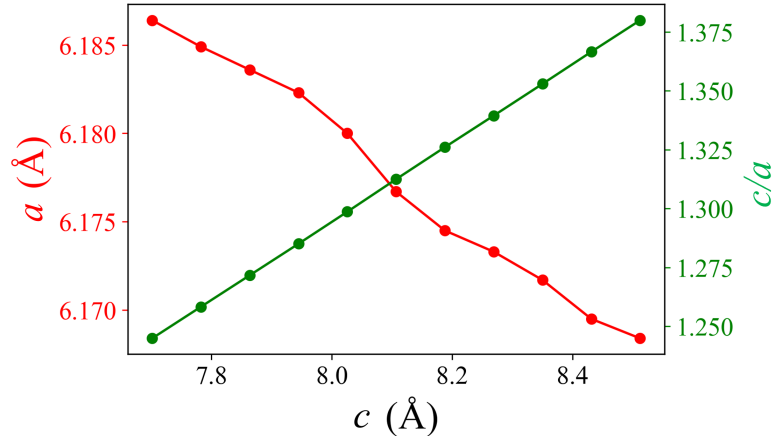


Figure S2: Calculated in-plane lattice parameter (a) and the c/a ratio as a function of out-of-plane lattice parameter (c).

III. COMPARISON BETWEEN PBE+SOC AND HSE06+SOC FUNCTIONALS

We have computed the band structures of $R3m$ phase of KIO_3 using semi-local Perdew-Burke-Ernzerhof (PBE) and non-local Heyd-Scuseria-Ernzerhof (HSE06) exchange-correlation (ϵ_{xc}) functional with spin-orbit coupling (SOC). Fig. S3a and S3b show the band structures calculated using PBE+SOC and HSE06+SOC, respectively. A slightly indirect band gap of 2.24 and 3.27 eV is observed using PBE+SOC and HSE06+SOC, respectively, at k -point A. Rashba spin splitting energy (δE), offset momentum (δk) along A-H and A-L directions, Rashba coefficient (α_R) and Dresselhaus coefficient (α_D) at conduction band minimum (CBM) are compared using both functionals in Table S1. Since Rashba parameters are comparable using both functionals, we have used PBE+SOC for further calculations being more cost effective. In addition, we have also compared the spin textures computed using PBE+SOC with HSE06+SOC (see Fig. S4). We have used uniformly space same dense k -grid for the comparison,. The spin textures computed using both functionals are in close agreement, However, there is small inconsistencies near the center. This can be removed by taking more dense k -grid near the center.

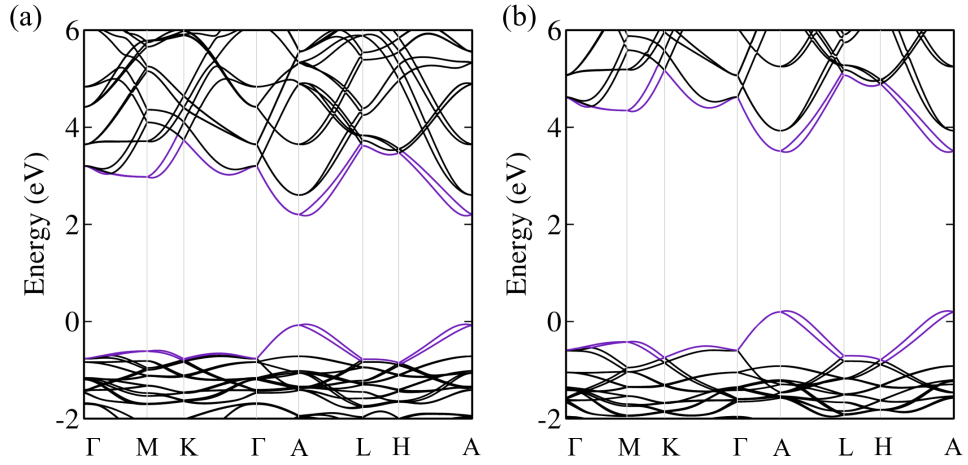


Figure S3: Band structure for $R3m$ phase of KIO_3 calculated using (a) PBE+SOC and (b) HSE06+SOC. The Fermi energy is set to VBM.

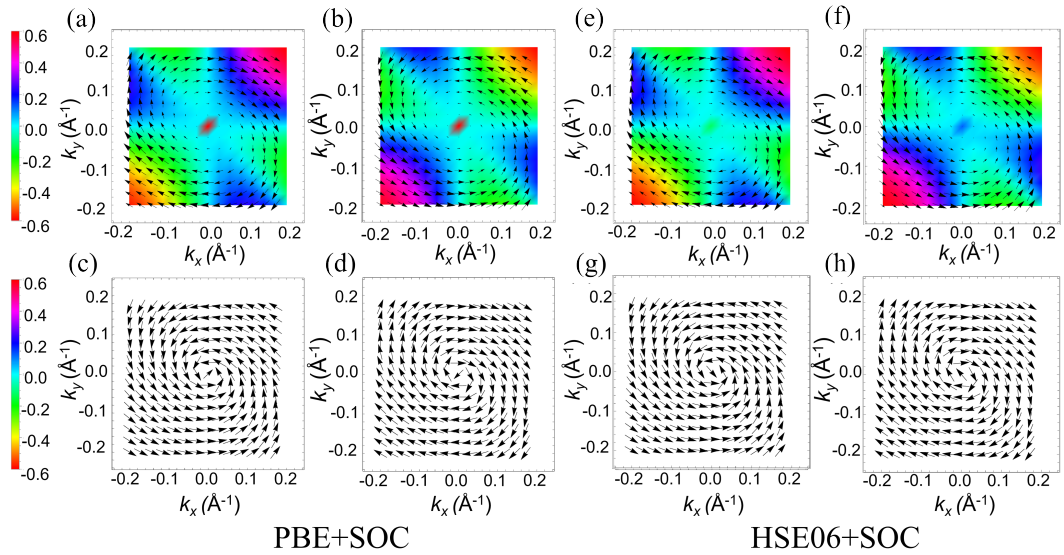


Figure S4: (a)-(b) Spin textures of two lowest conduction bands and (c)-(d) two uppermost of valence bands around the k -point A obtained using PBE+SOC. Similarly, [(e)-(h)] are the counterparts of [(a)-(d)] obtained using HSE06+SOC.

TABLE S1: Rashba parameters for conduction band-splitting at k -point A for $R3m$ phase.

ϵ_{xc} functional	δE (meV)	δk (\AA^{-1})	α_R (eV \AA)
PBE+SOC	27.3	0.047	1.16
HSE06+SOC	28.1	0.048	1.17

IV. TWO-BAND $k.p$ HAMILTONIAN

We aim at deriving the symmetry adapted two-band effective model Hamiltonian around k -point A. All those terms are included which are invariant under symmetry group operation, i.e., $O^\dagger H(\mathbf{k})O = H(\mathbf{k})$. Here, O represents the symmetry group operations belonging to the group of wave vectors and time-reversal operations. It is noteworthy that the considered $k.p$ Hamiltonian includes only spin degrees of freedom and does not take into account the orbital degrees of freedom. We have incorporated all the terms of the form $k_\alpha^n \sigma_\beta$, where k_α and σ_β are the crystal momenta and Pauli spin matrices, respectively, along with the free particle Hamiltonian $H_o(k)$. Since the time-reversal operator transforms k_α to $-k_\alpha$ and σ_β to $-\sigma_\beta$, the terms which are odd in momentum space, are only allowed to hold the time-reversal symmetry. Thus, the general expression of two-band $k.p$ model can be written as

$$H(\mathbf{k}) = H_o(\mathbf{k}) + \sum k_\alpha^n \sigma_\beta \quad (1)$$

where $\alpha, \beta = x, y, z$ and n takes only odd positive integers. In this model, for the specific case of k -point A, we have included upto cubic terms in crystal momentum, i.e., $k_x \sigma_x, k_x \sigma_y, k_x \sigma_z, k_y \sigma_x, k_y \sigma_y, \dots, k_z^3 \sigma_z$. Point group symmetry at k -point A is C_{3v} , which can be generated by trivial identity operation (E), three fold rotation about z -axis ($C_{3z} = e^{-i\pi/3\sigma_z}$) and mirror plane reflection in y - z plane ($M_x = i\sigma_x$) [1]. Transformation rules for σ_β and k_α under C_{3v} point group and time-reversal operations are summarized in Table S2. Thus, the constructed Hamiltonian

TABLE S2: The transformations of $(\sigma_x, \sigma_y, \sigma_z)$ and (k_x, k_y, k_z) with respect to the generators of the C_{3v} point group and time-reversal operator (T). Note that the generators C_{3z} and M_x are enough to form the whole group of C_{3v} . Hence, only these generators with time-reversal $T = i\sigma_y K$ operation (K is complex conjugation operator) are considered to construct the $k.p$ model for the k -point A.

	$C_{3z} = e^{-i\pi/3\sigma_z}$	$M_x = i\sigma_x$	$T = i\sigma_y K$
k_x	$-k_x/2 + \sqrt{3}k_y/2$	$-k_x$	$-k_x$
k_y	$-\sqrt{3}k_x/2 - k_y/2$	k_y	$-k_y$
k_z	k_z	k_z	$-k_z$
σ_x	$-\sigma_x/2 + \sqrt{3}\sigma_y/2$	σ_x	$-\sigma_x$
σ_y	$-\sqrt{3}\sigma_x/2 - \sigma_y/2$	$-\sigma_y$	$-\sigma_y$
σ_z	σ_z	$-\sigma_z$	$-\sigma_z$

can be written as

$$H_A(\mathbf{k}) = H_o(\mathbf{k}) + H_{SO} \quad (2)$$

where,

$$H_{SO} = \alpha \sigma_y k_x + \beta \sigma_x k_y + \gamma \sigma_z f(k_x, k_y) \quad (3)$$

and $H_o(\mathbf{k})$ is free particle Hamiltonian. Here, α, β are the coefficients of linear terms and γ is the coefficient of cubic term in SOC Hamiltonian. The linear Rashba and Dresselhaus Hamiltonian are given by $\alpha_R(\sigma_x k_y - \sigma_y k_x)$ and $\alpha_D(\sigma_x k_y + \sigma_y k_x)$, respectively [2]. Here, α_R and α_D are linear Rashba and Dresselhaus coefficients, respectively, which depend upon the properties of materials. The function $f(k_x, k_y)$, which has cubic dependence on crystal momentum, is given by

$$f(k_x, k_y) = (k_x^3 + k_y^3) - 3(k_x k_y^2 + k_y k_x^2) \quad (4)$$

Writing the Hamiltonian in matrix representation

$$H_A(\mathbf{k}) = \begin{pmatrix} E_0(\mathbf{k}) - \gamma f & \beta k_y - i\alpha k_x \\ \beta k_y - i\alpha k_x & E_0(\mathbf{k}) - \gamma f \end{pmatrix} \quad (5)$$

where the $E_0(\mathbf{k}) = \frac{\hbar^2 k_x^2}{2m_x} + \frac{\hbar^2 k_y^2}{2m_y}$ is the energy eigenvalue of free particle Hamiltonian. On diagonalizing the Hamiltonian, i.e, matrix in Eq. 5, gives

$$E(\mathbf{k})^\pm = E_0(\mathbf{k}) \pm \sqrt{\alpha^2 k_x^2 + \beta^2 k_y^2 + \gamma^2 f^2(k_x, k_y)} \quad (6)$$

and the corresponding spinor eigenfunctions are given by

$$\Psi_{\mathbf{k}}^\pm = \frac{e^{i\mathbf{k}\cdot\mathbf{r}}}{\sqrt{2\pi(\rho_\pm^2 + 1)}} \begin{pmatrix} \frac{i\alpha k_x - \beta k_y}{\gamma f(k_x, k_y) \mp E_{SO}} \\ 1 \end{pmatrix} \quad (7)$$

where $\rho_\pm^2 = \frac{\alpha^2 k_x^2 + \beta^2 k_y^2}{(\gamma f(k_x, k_y) \mp E_{SO})^2}$ is normalization constant, $E_{SO} = |E(\mathbf{k}) - E_0(\mathbf{k})|$ is the absolute energy eigenvalue of spin-orbit coupling Hamiltonian. Spin textures can be computed using the expectation values of spin operators. Using the fact that $S_i = \frac{\sigma_i}{2}$, expectation values of S_i ($s_i = \langle S_i \rangle$) are given by

$$\{s_x, s_y, s_z\}^\pm = \frac{1}{2} \{ \langle \sigma_x \rangle^\pm, \langle \sigma_y \rangle^\pm, \langle \sigma_z \rangle^\pm \} = \pm \frac{1}{E_{SO}} \{ \beta k_y, \alpha k_x, \gamma f(k_x, k_y) \} \quad (8)$$

where $\langle \sigma_i \rangle^\pm = \langle \Psi_{\mathbf{k}}^\pm | \sigma_i | \Psi_{\mathbf{k}}^\pm \rangle$ are the expectation values of the spin operators. Using Eq. 4 and 8, we can say that the three-fold degeneracy of out of plane spin texture (S_z) is a consequence of cubic term $f(k_x, k_y)$. The out of plane spin component is zero, when $S_z = 0$ or $f(k_x, k_y) = 0$. The lines $L_1: k_y = -k_x$, $L_2: k_y = 2x - \sqrt{3}x$ and $L_3: k_y = 2x + \sqrt{3}x$ in the momentum space are the directions of out of plane spin component. Slope of the lines L_1 , L_2 and L_3 are -1 , $2-\sqrt{3}$ and $2+\sqrt{3}$, respectively. Angle between two lines of slopes m_1 and m_2 can be computed using $\theta = \tan^{-1} \left| \frac{m_1 - m_2}{1 + m_1 m_2} \right|$. It is straightforward to see that smaller angle between any two lines is 60° , confirming the existence of three-fold degeneracy.

The linear Rashba (LR) Hamiltonian is given by $\alpha_R(\sigma_x k_y - \sigma_y k_x)$. The energy dispersion curves of LR splitted bands are given by $E_\pm = \hbar^2 k^2 / 2m \pm \alpha_R k$. This energy dispersion relation leads to shift in degenerate bands from high symmetry point by the offset momentum (δk). For k -points Γ and A , $k_x = k_y = 0$ and k_z is constant within the $k_x - k_y$ plane. Therefore, $\hbar^2 k_z^2 / 2m + \alpha_R k_z$ is taken to be constant and neglected in further calculations. Suppose we are calculating α_R in k_x direction and δk is offset momentum along k_x direction, then α_R can be estimated as follows

$$E_\pm = \hbar^2 k_x^2 / 2m \pm \alpha_R k_x \quad (9)$$

E_\pm have minimum energy (E_{min}) at offset momentum $\mp \delta k$. Rashba spin splitting energy (δE) is $E_{min} - E_{A/\Gamma}$. Thus, α_R can be estimated by approximating δE and δk using DFT and given by

$$\alpha_R = \frac{2\delta E}{\delta k} \quad (10)$$

Eq. 10 is used when there is pure LR effect.

Our considered SOC Hamiltonian ($H_{SO} = \alpha\sigma_y k_x + \beta\sigma_x k_y + \gamma\sigma_z[(k_x^3 + k_y^3) - 3(k_x k_y^2 + k_y k_x^2)]$) differs from LR Hamiltonian. Thus, possibility of splitting coming from linear Dresselhaus (LD) and cubic terms (cubic in k) are also taken in account. Energy eigenvalues corresponding to H_{SO} are given by $E_{SO}(\mathbf{k}) = \sqrt{\alpha^2 k_x^2 + \beta^2 k_y^2 + \gamma^2 f^2(k_x, k_y)}$, where $f(k_x, k_y) = (k_x^3 + k_y^3) - 3(k_x k_y^2 + k_y k_x^2)$. Initially, we have fitted the band structures along k_x direction using the relation $E_{SO}(\mathbf{k}) = \sqrt{\alpha^2 k_x^2 + \gamma^2 k_x^6}$. Since our considered range for DFT band structure is $|k_x| \leq 0.125 \text{ \AA}^{-1}$, $|\alpha k_x| \gg |\gamma k_x^3|$. Thus, we have estimated the values of α and β using the parametric fitting of DFT band structures along k_x and k_y directions, respectively. γ is estimated using the z -component of spin texture since it comes from cubic terms of H_{SO} . Moreover, overall band fitting including the cubic terms is also compared with only linear terms and are in well agreement. The H_{SO} can be written as linear combinations of LR and LD, which is given by the following expression

$$H_{SO}(\mathbf{k}) = H_R + H_D = \alpha\sigma_y k_x + \beta\sigma_x k_y = (\alpha_R + \alpha_D)\sigma_y k_x + (\alpha_D - \alpha_R)\sigma_x k_y \quad (11)$$

Using the α and β , we can estimate the values of α_R and α_D . Since $\alpha_D \simeq 0$, the splitting mainly comes from the LR effect. Therefore, the α_R calculated using the standard DFT ($\frac{2\delta E}{\delta k}$) and band fitting ($\frac{\alpha - \beta}{2}$) are found to be consistent with each other.

V. FOUR-BAND $\mathbf{k}\cdot\mathbf{p}$ HAMILTONIAN

The four-band $\mathbf{k}\cdot\mathbf{p}$ Hamiltonian including spin and orbital degrees of freedom is derived to understand the splitting around k -point A in $R3c$ phase. The representation of point group appropriate to spin-1/2 particles is usually determined by a group of double the order of the point group under consideration, known as the double group. The point group of wave vector associated with the k -point A is C_{3v} . The character table of double group corresponding to C_{3v} point group is given by Table S3. The number of conjugacy classes and irreducible representations (IR) (denoted by Γ_i) are 6. The lowest conduction band is two-fold degenerate at k -point A (see Fig. 4 upper panel in main manuscript) and corresponds to IR Γ_3 (representing the orbital degree of freedom). The inclusion of SOC leads to the splitted four bands around k -point A and degenerate at k -point A (see Fig. 4 lower panel in main manuscript). On including SOC, lowest conduction bands at k -point A correspond to direct product of Γ_3 and Γ_4 . IR Γ_4 represents the spin degrees of freedom. Using this, four-band $\mathbf{k}\cdot\mathbf{p}$ model is constructed employing the basis ($|x\uparrow\rangle$, $|x\downarrow\rangle$, $|y\uparrow\rangle$, $|y\downarrow\rangle$). The transformation rules of $(\sigma_x, \sigma_y, \sigma_z)$, $(\gamma_x, \gamma_y, \gamma_z)$ and (k_x, k_y, k_z) are given in Table S4 [3]. σ_i and γ_j are both Pauli matrices signifying the spin and orbital degrees of freedom, respectively. We have used the Hamiltonian, which is invariant under the operations C_{3z} , M_x and T and is given by

$$H_A(k) = \alpha(k_x^2 + k_y^2) + \beta(k_x^2 + k_y^2)^2 + \delta(k_x^2 + k_y^2)^3 + \eta[(k_x^2 - k_y^2)\gamma_z + 2k_x k_y \gamma_x] + [\Delta + \Lambda(k_x^2 + k_y^2) + K(k_x^2 + k_y^2)^2]\gamma_y \sigma_z + [\kappa + \zeta(k_x^2 + k_y^2)](k_x \sigma_y - k_y \sigma_x) + \lambda k_x (k_x^2 - 3k_y^2)\sigma_z + \xi k_x (k_x^2 - 3k_y^2)\gamma_z + \rho[(k_x \gamma_x - k_y \gamma_z)\sigma_x - ((k_y \gamma_x - k_x \gamma_z)\sigma_y)] \quad (12)$$

Here, α , β , δ , η , Δ , Λ , K , κ , ζ , ξ and ρ are coefficients signifying the strength of splitting. The terms having coefficients α , β and δ are the effective mass terms. The term with coefficients η and ξ includes only orbital degrees of freedom. Spin degrees of freedom are taken into account with the terms containing κ , ζ and λ . The remaining terms with coefficients Δ , Λ , K and ρ couple the orbital and spin degrees of freedom. The coupling terms are responsible for the novel spin textures observed around k -point A in $R3c$ phase (see Fig. 4i-l in main manuscript). Alongside of full four-band $\mathbf{k}\cdot\mathbf{p}$ Hamiltonian, we have constructed a modified Hamiltonian to understand the importance of orbital degrees of freedom in four-band $\mathbf{k}\cdot\mathbf{p}$ Hamiltonian. The modified Hamiltonian excludes the terms containing the Pauli matrices, which signify the orbital degrees of freedom from four-band $\mathbf{k}\cdot\mathbf{p}$ Hamiltonian ($\eta = \xi = \Delta = \Lambda = K = \rho = 0$). Fig. 5d in main manuscript shows lowest conduction bands around k -point A using DFT and modified Hamiltonian. The band structure (Fig. 5d in main manuscript) obtained using modified Hamiltonian deviates from the DFT band structure. This signifies the importance of the full four-band $\mathbf{k}\cdot\mathbf{p}$ Hamiltonian. The Hamiltonian without the terms containing orbital degrees of freedom cannot reproduce the band dispersion and spin textures observed around k -point A.

TABLE S3: Character table of double group corresponding to C_{3v} point group. Under \bar{E} operation, the sign of spinor gets reversed. S_x , S_y and S_z represent the axial vectors. The \uparrow and \downarrow represents the spin-up and spin-down states of the spinor.

	E	\bar{E}	$2C_3$	$2\bar{E}C_3$	$3\sigma_v$	$3\bar{E}\sigma_v$	Basis functions
Γ_1	1	1	1	1	1	1	z
Γ_2	1	1	1	1	-1	-1	S_z
Γ_3	2	2	-1	-1	0	0	$(x, y), (S_x, S_y)$
Γ_4	2	-2	1	-1	0	0	(\uparrow, \downarrow)
Γ_5	1	-1	-1	1	i	-i	—
Γ_6	1	-1	-1	1	-i	i	—

TABLE S4: The transformations of $(\sigma_x, \sigma_y, \sigma_z)$, $(\gamma_x, \gamma_y, \gamma_z)$ and (k_x, k_y, k_z) with respect to generators of the C_{3v} point group and time-reversal operator (T). Note that the generators C_{3z} and M_x are enough to form the whole group of C_{3v} . Hence, only these generators with time-reversal operation $T=i\sigma_yK$ (K is complex conjugation operator) are considered to construct the $\mathbf{k}\cdot\mathbf{p}$ model for k -point A.

	$C_{3z}=e^{-i\pi/3\sigma_z}$	$M_x=i\sigma_x$	$T=i\sigma_yK$
k_x	$-k_x/2+\sqrt{3}k_y/2$	$-k_x$	$-k_x$
k_y	$-\sqrt{3}k_x/2-k_y/2$	k_y	$-k_y$
k_z	k_z	k_z	$-k_z$
σ_x	$-\sigma_x/2+\sqrt{3}\sigma_y/2$	σ_x	$-\sigma_x$
σ_y	$-\sqrt{3}\sigma_x/2-\sigma_y/2$	$-\sigma_y$	$-\sigma_y$
σ_z	σ_z	$-\sigma_z$	$-\sigma_z$
γ_x	$-\gamma_x/2+\sqrt{3}\gamma_z/2$	$-\gamma_x$	γ_x
γ_y	γ_y	$-\gamma_y$	$-\gamma_y$
γ_z	$-\sqrt{3}\gamma_x/2-\gamma_z/2$	γ_z	γ_z

VI. RASHBA PARAMETERS FOR SELECTED BULK FERROELECTRIC MATERIALS

In the Table S5, we have compared the Rashba coefficients (α_R) of some well known bulk ferroelectric materials with the bulk KIO_3 . Space group symmetry is also included with the material. For hafnia (HfO_2), δE and δk are not provided in the literature. All the values are reported upto respective significant Figures in the references and may not be consistent with each other.

TABLE S5: Rashba spin splitting energy (δE), offset momentum (δk) and Rashba coefficient (α_R) of some selected bulk ferroelectric materials.

Material	Space group	δE (meV)	δk (\AA^{-1})	α_R (eV \AA)	Reference
KIO_3	$R3m$	23.2	0.053	1.16	This work
KIO_3	$R3c$	14.8	0.047	0.78	This work
BiAlO_3	$R3c$	7.34	0.04	0.39	[4]
BiAlO_3 (along Z-R)	$P4mm$	9.40	0.03	0.74	[4]
BiAlO_3 (along A-Z)	$P4mm$	8.62	0.03	0.65	[4]
LaWN_3	$Pna2_1$	2.20	0.014	0.31	[5]
LaWN_3	$R3c$	3.49	0.051	0.18	[5]
BiInO_3	$Pna2_1$	130	0.19	1.91	[3]
PbTiO_3	$P4mm$	5.45	0.50	0.51	[6]
HfO_2	$Pca2_1$	-	-	0.06	[7]
KMgSb	$P6_3mc$	10	0.024	0.83	[8]
LiZnSb	$P6_3mc$	21	0.023	1.82	[8]
β -(MA) PbI_3	$P4mm$	12	0.015	1.5	[9]
β -(MA) SnI_3	$P4mm$	11	0.011	1.9	[9]
GeTe	$R3m$	227	0.09	4.8	[10]

[1] Bilbao Crystallographic Server, Generators and general positions, https://www.cryst.ehu.es/cryst/get_gen.html.

[2] L. Tao and E. Y. Tsymbal, *J. Phys. D: Appl. Phys.*, 2021, **54**, 113001.

[3] L. Tao and E. Y. Tsymbal, *Nat. Commun.*, 2018, **9**, 1–7.

[4] L. G. D. da Silveira, P. Barone and S. Picozzi, *Phys. Rev. B*, 2016, **93**, 245159.

[5] S. Bandyopadhyay, A. Paul and I. Dasgupta, *Phys. Rev. B*, 2020, **101**, 014109.

- [6] R. Arras, J. Gosteau, H. Zhao, C. Paillard, Y. Yang and L. Bellaiche, *Phys. Rev. B*, 2019, **100**, 174415.
- [7] L. Tao, T. R. Paudel, A. A. Kovalev and E. Y. Tsybal, *Phys. Rev. B*, 2017, **95**, 245141.
- [8] A. Narayan, *Phys. Rev. B*, 2015, **92**, 220101.
- [9] M. Kim, J. Im, A. J. Freeman, J. Ihm and H. Jin, *Proc. Natl. Acad. Sci.*, 2014, **111**, 6900–6904.
- [10] D. Di Sante, P. Barone, R. Bertacco and S. Picozzi, *Adv. Mater.*, 2013, **25**, 509–513.